PAPER • **OPEN ACCESS**

Transparent neutral-colored $CsPbBr_3$ perovskite solar cell with biological soybean lecithin food additives

To cite this article: Diksha Thakur *et al* 2026 *Nanotechnology* **37** 055401

IOP Publishing Nanotechnology 37 (2026) 055401 https://doi.org/10.1088/1361-6528/ae3765

Nanotechnology

PAPER

Transparent neutral-colored $CsPbBr_3$ perovskite solar cell with biological soybean lecithin food additives

Diksha Thakur[1,4], **Davide Santucci**[1,4], **Suresh K Podapangi**[2,4], **Francesca Pallini**[3], **Jie Xu**[1], **Antonio Cricenti**[2], **David Becerril Rodriguez**[2], **Marco Luce**[2], **Sathy Harshavardan Reddy**[1], **Mauro Sassi**[3], **Fabio Matteocci**[1], **Aldo Di Carlo**[1,2] and **Thomas M Brown**[1,*]

[1] CHOSE (Centre for Hybrid and Organic Solar Energy), Department of Electronic Engineering, Tor Vergata University of Rome, Via del Politecnico 1, 00133 Rome, Italy
[2] Institute for Structure of Matter, National Research Council (CNR-ISM), 00133 Rome, Italy
[3] Department of Materials Science, University of Milano-Bicocca, Via R. Cozzi 55, I-20125 Milan, Italy
[4] D. Thakur, D Santucci and S K Podapangi contributed equally to the work.
[*] Author to whom any correspondence should be addressed.

E-mail: thomas.brown@uniroma2.it

Keywords: transparent, perovskite solar cell, lecithin additive, color neutral

Supplementary material for this article is available online

OPEN ACCESS

RECEIVED
29 February 2024

REVISED
19 December 2025

ACCEPTED FOR PUBLICATION
13 January 2026

PUBLISHED
3 February 2026

Abstract

We report the first perovskite solar cell incorporating soybean lecithin, a biological plant-based food additive. When added in small concentration to perovskite precursor inks, it helps to obtain compact and uniform $CsPbBr_3$ thin films. Our devices exhibit very high average visible transmittances (AVTs) (>70%), color rendering index (CRI) up to 84% and neutrality (CIE coordinates of 0.38, 0.39). The addition of lecithin almost doubled power conversion efficiency from 0.84% to 1.52%. Such high transparency, although limiting their overall efficiency, can be used in environments where transparency and color neutrality are important features, such as windows, facades, lens in smart glasses, and greenhouses. The transparency-efficiency profile fits the trend in performance of emerging photovoltaic devices, with amongst the highest voltages reported at these transmittances. Furthermore, the stability in ambient air also improved with addition of lecithin, losing only 25% of efficiency after 1 year versus 50% for devices with no lecithin.

1. Introduction

Perovskite solar cells (PSCs) are a promising photovoltaic (PV) technology because of their high power conversion efficiency, low-cost materials and simple solution processing methods [1, 2]. However, long-term stability remains a significant challenge that continues to impede their commercialization [3–5]. Among various perovskite compositions, the $CsPbBr_3$ all-inorganic perovskite exhibits superior thermal, moisture and photo stability compared to its organic-inorganic counterparts, owing to the absence of volatile organic cations [6]. Its high transmissivity and high CRI make it suitable for use in semi-transparent and tandem PV [6–8]. Furthermore, $CsPbBr_3$'s wide bandgap (∼2.3 eV) and high visible transmittance make it a promising material for semi-transparent and building-integrated photovoltaic (BIPV) applications. Recent studies have demonstrated semi-transparent $CsPbBr_3$ solar cells with power conversion efficiencies (PCEs) of up to ∼6% and AVT of 55%–60%, achieved through optimized film morphology and transparent electrodes [9]. When transparency exceeds 70%, most reported perovskite devices show PCEs ∼1% [10, 11].

Obtaining uniform and compact films for $CsPbBr_3$ by solution processing is challenging due to the solubility difference of CsBr and $PbBr_2$ in solvents like dimethyl sulfoxide (DMSO), often resulting in poor film quality. This has limited the development of efficient $CsPbBr_3$ solar cells through spin-coating, without the use of vapor deposition methods [4, 12]. To overcome these challenges, several fabrication

strategies have been explored to improve film quality and device performance. Multistep deposition is the most common route to fabricate high-quality $CsPbBr_3$ films. In the earliest $CsPbBr_3$ device report, Gupta *et al* demonstrated ∼6% PCE on mesoporous TiO_2 using solution processing, establishing the baseline for this all-inorganic absorber [7]. Building on this work, still not focusing on transparency, Liu *et al* used a modified multistep spin-coating strategy with interface engineering to achieve 8.79% in carbon-electrode $CsPbBr_3$ cells, highlighting the film-quality advantages of the sequential route [13]. More recently, Zhou *et al* introduced CsCl-doped SnO_2 as a buried-interface passivation layer to promote ordered crystal growth and optimize energy alignment; with a carbon electrode, they reported a champion 11.16% PCE and $V_{OC} \approx 1.68$ V [14].

In parallel, the simplified one-step spin-coating method remains attractive for its scalability and high throughput, although it is rapid crystallization often produces rougher films and lower device performance compared to multistep routes. Only a few reports are available on one-step spin-coating of $CsPbBr_3$; however, film quality and device performance have been notably improved through the incorporation of additive compounds and solvent engineering strategies [15, 16]. A wide range of organic and inorganic additives have been employed to modulate nucleation and crystal growth dynamics, passivate defects, and enhance film compactness in PSCs. Inorganic additives, such as alkali metal ions (e.g., Li^+, Na^+, K^+, Cs^+, and Rb^+) and halide salts (e.g., KI, NaI), have been shown to improve structural and thermal stability, suppress ion migration, and enhance charge transport [17–21]. Alkali metal ions, in particular, have been found to reduce ion migration in perovskite materials by mitigating adverse interfacial recombination pathways, thereby stabilizing the open-circuit voltage [17]. Organic additives, such as DMSO, urea, thiourea, alkylammonium salts and fullerenes (e.g., C_{60}, PCBM) facilitate controlled perovskite crystallization, resulting in larger grain sizes (especially with Lewis base additives), minimized pinhole formation, reduced trap-state densities, and enhanced device stability [22–25].

In recent years, bio-based additives have gained attention as eco-friendly alternatives to conventional synthetic additives [26–30]. These include naturally derived compounds such as amino acids, phospholipids, and polysaccharides, which can coordinate with metal cations in the precursor and facilitate film formation, defect passivation, and grain boundary stabilization [22, 26–29]. In conventional organic-inorganic perovskites, bio-compounds (like succinate and DNA) have been shown to help passivate defects, making devices more efficient and stable, similarly to organic PV [31–34]. Bio-additives such as cellulose acetate have been used in $CsPbIBr_2$ based PSCs to control the crystallization process and produce homogeneous, pinhole-free perovskite films [35] Moreover, other organic additives including polyethylene glycol, polyvinylpyrrolidone, and isobutyramide have been employed in $CsPbBr_3$ solar cells to enhance film crystallinity by modulating nucleation and crystallization dynamics, while simultaneously passivating defects [35, 36]. Lecithin has been used as a surface-capping ligand in the synthesis of $CsPbBr_3$ nanocrystal [37, 38] and to improve the electroluminescence and photoluminescence stability of $CsPbBr_3$ based LEDs (light-emitting diodes) [39, 40]. Fabricating uniform $CsPbBr_3$ thin films is particularly challenging due to the solubility differences between CsBr and $PbBr_2$ in DMSO. To address this, lecithin was added to the precursor solution to regulate nucleation and crystal growth of the perovskite thin films. Additionally, low-temperature annealing for a short duration was performed to control the solvent evaporation rate and, consequently, the crystal growth of the perovskite thin films. Here for the first time, we show that this mass-produced, natural and commercial food product, incorporated in the bulk of the $CsPbBr_3$, leads to significant improvement in both efficiency and stability in highly-transparent neutral-colored solar cells.

2. Experimental details

The architectures of our devices were glass/FTO/c–TiO_2 (compact TiO_2)/m-TiO_2 (mesoporous TiO_2)/$CsPbBr_3$ + lecithin (Lec)/Spiro-OMeTAD/Gold (Au). ITO replaced Au as top contact to make fully transparent solar cells. Glass/FTO (Pilkington, 12 Ω/□) substrates (patterned by laser ablation, cut in 2.5 cm × 2.5 cm size) were cleaned in ultrasonic bath with deionized water, ethanol, acetone, 2-propanol, and again ethanol (25 °C, 15 min each). Substrates were exposed to compressed air and UV-Ozone treatment (15 min). The c-TiO_2 was deposited by spray pyrolysis at 460 °C from a precursor solution of titanium diisopropoxide bis(acetylacetonate) (75% iPrOH), acetylacetone, and ethanol (3:2:45 volume ratio) with 10 spray cycles. The m-TiO_2 was deposited by spin coating (3000 rpm, 15 s) Dyesol 30 NRD titania nanoparticle paste in ethanol (1:4 mass ratio). Lecinova, a food product majorly composed of soybean lecithin, was ground into a fine powder using a mortar and then mixed with DMSO at a concentration of 20 mg ml^{-1}. Overnight stirring and filtering (0.45 μm) occurred

before mixing the Lec-DMSO solution with $CsPbBr_3$ precursor ink (0.22 mmol of CsBr from Sigma–Aldrich and 0.2 mmol $PbBr_2$ from Tokyo Chemical Industry Co dissolved in 1 ml of DMSO). The lecithin solution (Lec-DMSO) was added to $CsPbBr_3$ precursor ink in different volume percentages of 0% (reference), 1%, 3% and 5%. The solution was stirred followed by filtering, and then the deposition was carried out in a nitrogen-filled glovebox by spin-coating (100 μl of $CsPbBr_3$ + Lec ink, 1500 rpm, 35 s) followed by annealing (90 °C, 3 min). Spiro-OMeTAD solution was prepared by dissolving the molecules in chlorobenzene (73.42 mg ml^{-1}) and stirred overnight. It was then doped with 16.6 μl ml^{-1} Li-TFSI (Lithium bis(trifluoromethanesulfonyl)imide) stock solution (530 mg ml^{-1} in acetonitrile), 26.77 μl ml^{-1} TBP (Tributyl phosphate) and 7.2 μl ml^{-1} cobalt (III) complex solution, and finally spin-coated on samples in a nitrogen-filled glovebox (2000 rpm, 20 s). The 100 nm thick Au electrode was deposited by thermal evaporation (10^{-6} mbar), the first 10 nm at 0.3 Å s^{-1}, and the other 90 nm at 1 Å s^{-1}. For fully transparent devices fabrication, a 160 nm layer of ITO was deposited instead of Au by magnetron sputtering ($1.1{\cdot}10^{-3}$ mBar and 60 W RF power). Silver paste was applied at the edges for connection to the measurement cables. PV measurements were carried out under ABET class A sun simulator with steps of 20 mV at scan rate of 100 mV s^{-1} (cells area of 0.09 cm^2) [41]. Dark J–V were measured with Arkeo-Ariadne, Cicci Research. Devices were stored in a box in air for determining stability after 1 year (ISOS-D-1 protocol, dark storage, ambient air, 23 ± 4 °C). Morphology pictures were taken by SEM (scanning electron microscopy) SUPRA 35 (Carl Zeiss SMT). An open source software ImageJ was used to analyze the SEM images to calculate the grain size distribution and percentage of surface coverage. Transmittance was measured with a Shimadzu UV-2550 spectrometer equipped with an integrating sphere. Transient photoluminescence was measured with an Edinburgh Instrument FLS980 spectrometer. PAN analytical empyrean x-ray diffractometer (XRD) analyzer was used at 40 kV with Cu Kα1α2radiation (λ = 1.5418 Å). The transmittance curves used to determine the CIE coordinate were measured with the UV spectrometer (Shimadzu UV-2550) equipped with integrated sphere and a combination of deuterium arc lamp (D2) and halogen lamp. The CIE chromaticity coordinates and CRI were determined under illumination from a combination of deuterium arc lamp (D2) and halogen lamps. The AVT, CRI, and CIE 1931 chromaticity coordinates were determined following the methodology outlined by Yang *et al* [42]. Specifically, the measured transmittance spectra of our devices were input into the calculation spreadsheet provided in the supplementary information of that paper, which implements the standard equations and weighting functions (photopic eye response and AM 1.5 G spectrum). The spreadsheet automatically computes AVT, CRI, and CIE chromaticity coordinates from the input spectra, ensuring consistency with the recommended best-practice protocol [42]. Fourier transform infrared (FTIR) spectroscopy measurements were performed in ATR (attenuated total reflectance) mode using a Nicolet iS20 FTIR spectrometer (thermo scientific) equipped with a smart iTX™ accessory. X-ray photoelectron spectroscopy (XPS) spectra were recorded in a Vacuum Generators VG-450 ultrahigh-vacuum chamber equipped with an Al K_α radiation source. The position of the Fermi level (E_F) was determined with an accuracy of 50 meV by photoemission from the metallic sample holder.

3. Results and discussion

We introduced lecithin (Lec)-DMSO volume percentages (0%–5%) in the $CsPbBr_3$ perovskite precursor ink and fabricated glass/FTO/c–TiO_2/m–TiO_2/$CsPbBr_3$ + Lec/Spiro-OMeTAD/Au solar cells. Lecithin addition increased V_{OC} and J_{SC} significantly (table 1, figure 1(a)). 3% lecithin solution led to the largest improvement with the maximum PCE increasing from 0.84% to 1.52% (box plots are shown in figure S1). $CsPbBr_3$ solar cells fabricated on different TCOs (ITO and FTO) and ETLs (SnO_2 and TiO_2), both in planar and with mesoporous scaffolds, exhibit a consistent trend. The incorporation of lecithin even on glass/ITO/SnO_2/$CsPbBr_3$ + Lec/Spiro-OMeTAD/Au solar cells systematically increases PCE, with the maximum value (∼1.5%) achieved at 3% lecithin concentration, irrespective of the substrate and ETL. These results confirm the reproducible beneficial effect of lecithin across different device architectures.

Dark J–V curves figure (1(b)), show that leakage currents of cells made with 3% lecithin ink were ∼40 times lower compared to the 0% pristine $CsPbBr_3$. Shunt resistances R_{SH} also improved from $(1.3 \pm 0.1){\cdot}10^5\Omega$ to $(1.7 \pm 0.4){\cdot}10^5$ Ω. Series resistance R_S decreased from (770 ± 70) Ω to (580 ± 40) Ω at concentration 3%.

These improvements in R_S, R_{SH} and dark recombination currents explain the enhancements in PV parameters [43, 44] indicating effective passivation of defects by the lecithin additive. It not only improved PCE (by 72% and 81% for average and best cells respectively) but helped obtain more stable

Table 1. Average PV parameters with standard deviation of glass/FTO/c–TiO_2/m–TiO_2/ $CsPbBr_3$ + Lec/Spiro-OMeTAD/electrode solar cells as a function of volume % of lecithin solution added in the precursor. The 1st column provides lecithin concentration as well as the top electrode used. Values of the best cells are in brackets.

Electrode/lecithin %	V_{oc} (V)	J_{sc} (mA cm^{-2})	FF (%)	PCE (%)
Au/0%	0.66 ± 0.01 (0.66)	1.65 ± 0.13 (1.77)	70.4 ± 1.7 (72.5)	0.76 ± 0.05 (0.84)
Au/1%	0.70 ± 0.03 (0.74)	2.38 ± 0.35 (2.66)	68.0 ± 1.9 (68.8)	1.21 ± 0.08 (1.35)
Au/3%	0.75 ± 0.04 (0.79)	2.42 ± 0.24 (2.76)	69.0 ± 1.9 (69.7)	1.31 ± 0.12 (1.52)
Au/5%	0.79 ± 0.01 (0.80)	2.34 ± 0.20 (2.50)	68.0 ± 1.0 (69.1)	1.26 ± 0.10 (1.39)
ITO/3%	0.55 ± 0.09 (0.69)	2.12 ± 0.20 (2.40)	47.5 ± 6.3 (56.6)	0.57 ± 0.07 (0.67)

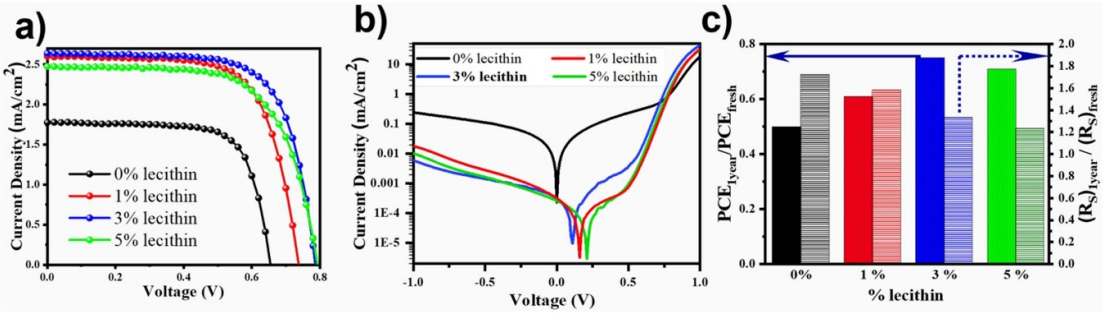

Figure 1. (a) Current density-voltage (J–V) curves of the best $CsPbBr_3$ solar cells fabricated with different lecithin solution volume percentages in the perovskite precursor inks; (b) dark J–V curves of best cells at different lecithin percentages. (c) Ratio of power conversion efficiencies (full bars) after 1 year compared to fresh ($PCE_{1\ year}$/ PCE_{fresh}) together with ratio of series resistances $(R_S)_{1\ year}/(R_S)_{fresh}$ (dashed bars) for each lecithin percentage.

devices. Figure 1(c) shows that 3% solar cells maintained 75% of initial PCE after ISOS-D-1 shelf-life tests [45] versus 50% maintained by those without (0% cells). Whereas R_{SH} after 1 year was in the range of $(1.0 \pm 0.2)\cdot10^5$ Ω for all cells, it was mostly R_S which accompanied degradation in performance (see ratios in figure 1(c)), with 0% having the largest value of $1.3\cdot10^3$ Ω compared to 3% with the lowest at $0.8\cdot10^3$ Ω. Thus, lecithin addition helps maintain the resistance through the layer and interfaces over time [46].

The surface morphology of perovskite thin films with varying lecithin concentrations (0%–5%) is presented in figure 2. The SEM images clearly indicate that increasing lecithin concentration leads to the enhanced surface coverage and film compactness, likely due to better loading of perovskite in mesoporous TiO_2. With lecithin additive the perovskite film envelopes the mesoporous TiO_2 layer more uniformly as illustrated in cross-sectional SEM images (figure 3). To improve the visualization of the layer stacking and thickness uniformity, an additional cross-sectional SEM image with a larger field of view has been included in the supporting information (figure S2). Furthermore, the grains become more well-defined with the incorporation of soyabean lecithin. This improved morphology leads to reduce charge recombination [44], thereby enhancing power conversion efficiency of the devices.

A previous study on LEDs has shown that crystallite size reduction, compactness and smoothness of $CsPbBr_3$ is due to lecithin coordinating with Cs^+ and Pb^{2+} cations in the precursor solution [39]. The domains with higher brightness in figure 2(c) appear to result from localized differences in film thickness and/or crystallinity. High resolution SEM images and grain size distribution plots, provided in the supplementary information file (figures S3 and S4), further confirm that the incorporation of soyabean lecithin leads to the formation of compact and well-covered films with well-defined grains. The surface coverage increases from 31% for the pristine film to 52% for the 3% lecithin and slightly decreases to 45% for the 5% lecithin. The addition of soybean lecithin enhances film morphology by promoting better domain organization and closer grain packing, likely due to a more controlled nucleation process. These morphological improvements are critical for achieving consistent device performance, particularly in devices with high AVT. To investigate why the devices operate effectively even when the perovskite films are not highly uniform, we fabricated control diodes (FTO/c–TiO_2/m–TiO_2/Spiro/Au) without any perovskite layer. As shown in figure S5, these diodes exhibit clear rectifying J–V characteristics under

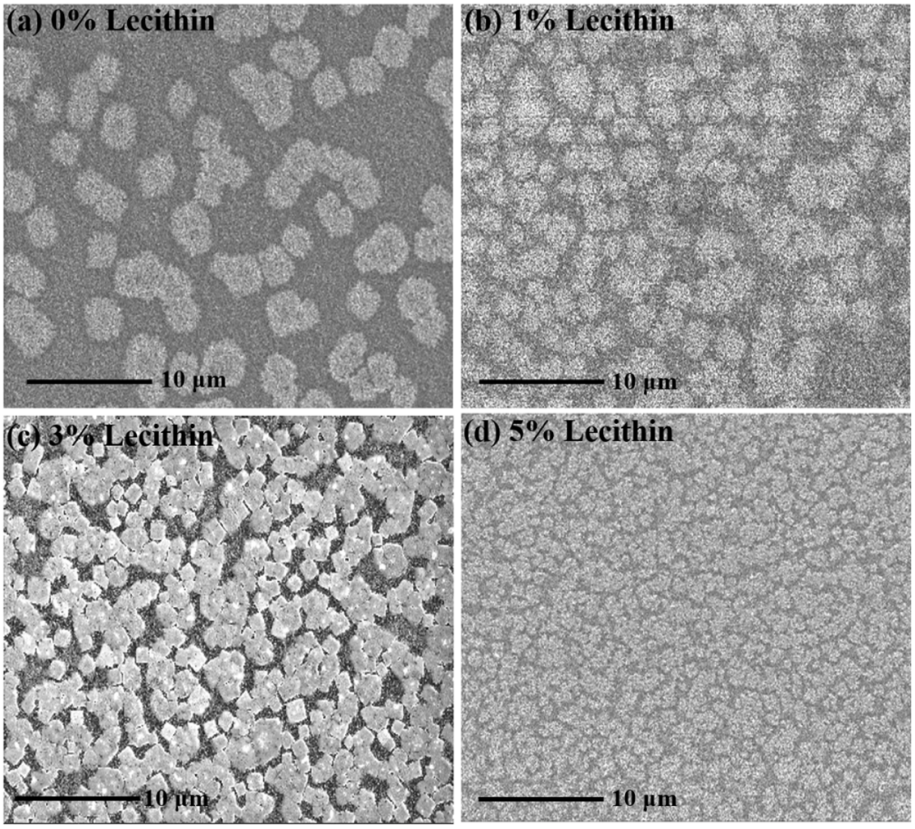

Figure 2. Top-view SEM images of $CsPbBr_3$ thin film with different concentration of lecithin with the following stack: glass/FTO/c-TiO_2/m-TiO_2/ $CsPbBr_3$ + Lec.

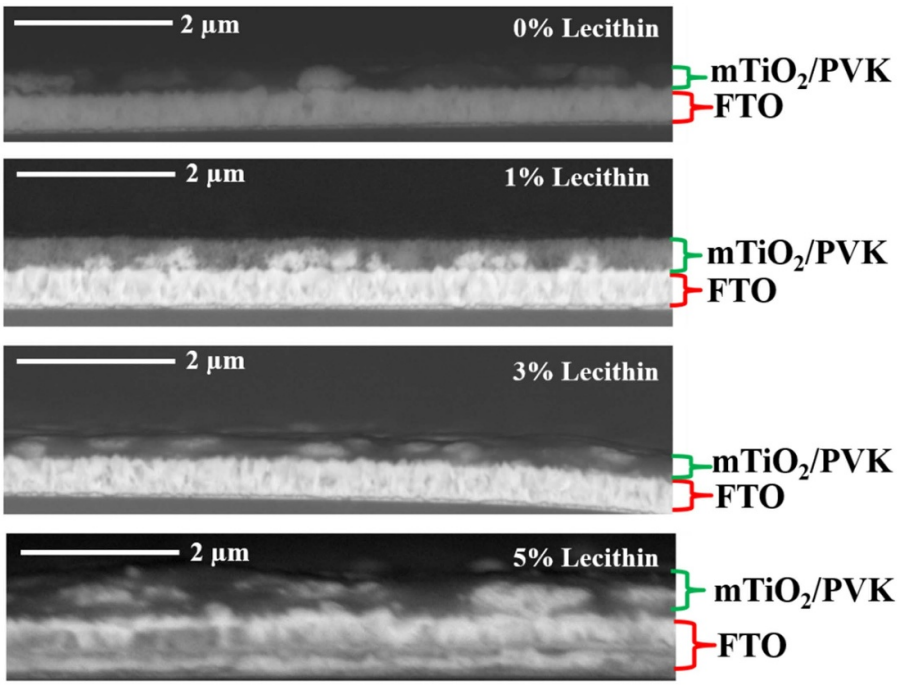

Figure 3. Cross-sectional SEM images of $CsPbBr_3$ thin films with different concentration of lecithin with the following stack: glass/FTO/c-TiO_2/m-TiO_2/ $CsPbBr_3$ + Lec.

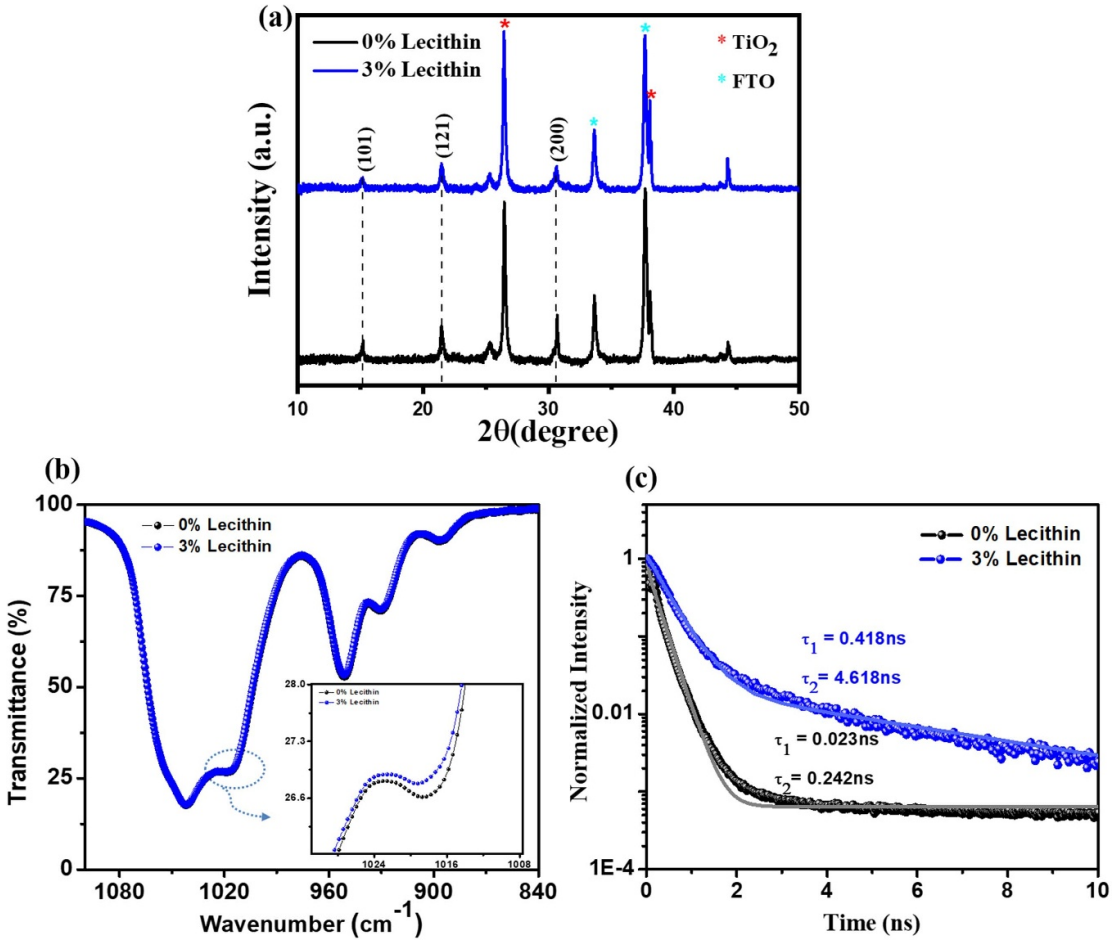

Figure 4. (a) X-ray spectra, (b) FTIR spectra and (c) time-resolved photoluminescence spectra with calculated lifetimes (tau) of $CsPbBr_3$ films with optimized concentration (3%) of lecithin and without (0%) lecithin.

one-sun illumination with an open circuit voltage as high as 0.6 V. The latter confirming that the c–TiO_2/m–TiO_2 multilayer transport stacks are of sufficient high quality to stop any possibile significant shunting occurring between the Spiro-OMeTAD/Au top layers and the bottom transparent TCO electrode.

The elevated series resistance (R_S) observed in our devices is primarily attributed to inefficient infiltration and incomplete loading of $CsPbBr_3$ within the mesoporous TiO_2 scaffold, which limits interparticle connectivity and hinders efficient electron percolation through the TiO_2 network. In contrast, non-uniform surface coverage generally reduces the shunt resistance (R_{SH}) by introducing leakage pathways rather than increasing R_S. Similar behavior has been previously reported in mesoscopic perovskite architectures, where insufficient pore filling and discontinuous perovskite coverage impede charge extraction and increase R_S [47–49] In addition, poor interface quality and contact resistance at both the perovskite/TiO_2 and perovskite/hole transport interfaces can contribute significantly to resistive losses within the device stack [14, 50].

The incorporation of soybean lecithin improves perovskite film morphology and infiltration uniformity (figures 2(b)–(d)), resulting in a more continuous and conformal perovskite layer that envelopes the mesoporous TiO_2 layer (figure 3) and improves interfacial contact. Organic additive molecules (lecithin belonging to this definition [39]) are known to regulate surface energy, slow crystallization, and enhance precursor wetting, thereby promoting uniform perovskite nucleation and improved charge-transport pathways [23–25, 39, 51]. Consequently, lecithin addition reduces both bulk and interfacial series resistances, leading to enhanced carrier extraction and improved overall device performance.

To understand the chemical interaction between lecithin and the perovskite precursor components, FTIR spectroscopy of $CsPbBr_3$ precursor solution in DMSO with and without lecithin is presented as figure 4(b). The characteristic peak at $\sim$ 1020 cm^{-1} corresponds to the S=O stretching vibration of DMSO, when in coordination with metal ions such as Cs+ and Pb^2+ [39, 52]. Upon the addition of lecithin, a slight increase in transmittance at this wavenumber is observed, suggesting that the S=O

bond vibrations are increasingly restricted. This increased transmittance can be interpreted as a sign that lecithin molecules compete with DMSO for coordinating with the metal cations, effectively displacing DMSO from its binding sites. As a result, fewer DMSO molecules are involved in metal–oxygen interactions, leading to weaker S=O vibrational signals.

This competitive coordination mechanism facilitates controlled nucleation during the film formation process. The strong interaction between lecithin and $CsPbBr_3$ promotes uniform crystallization, resulting in compact thin films with reduced defects and improved film quality.

The XRD spectra shows (see figure 4(a)) that lecithin is not altering $CsPbBr_3$ lattice, but mainly locates at grain boundaries [53] thus contributing to the passivation of defects [37]. Peaks located at 15.1°, 21.5°, 30.5° belong to (101), (121), (200) planes of orthorhombic $CsPbBr_3$ crystal [54]. Full width half maximum of these peaks increased from 0% to 3% (respectively from 0.22 to 0.32, from 0.25 to 0.29, from 0.25 to 0.27) confirming the smaller crystallites size at 3%, according the Scherrer equation [55]. Peaks at 26.5° and 37.7° are from the mesoporous TiO_2 [56]. In our study, although lecithin addition results in a modest decrease in average crystallite size (as determined from XRD), we observe a marked improvement in surface coverage figures (2(a) and (b)). We propose that these morphological improvements offset the negative impact of smaller grain size by effectively reducing shunting pathways and interfacial recombination centers.

Time-resolved photoluminescence (TRPL) spectra of the $CsPbBr_3$ thin film with optimized lecithin concentration is presented in figure 4(c). The TRPL decay curves were analyzed using a biexponential fitting model $I(t) = I_0 + A_1 e^{-(t-t_0)/\tau 1} + A_2 e^{-(t-t_0)/\tau 2}$, which is used here as a phenomenological approach to compare relative carrier recombination dynamics among different samples [57–59]. The fast component (τ_1) is generally attributed to surface or interfacial non-radiative recombination, while the slower component (τ_2) reflects bulk or trap-assisted recombination processes. This model does not represent the full physical recombination kinetics but provides a practical means to assess the influence of lecithin on recombination suppression and carrier lifetime extension [59]. The increased recombination lifetime (τ_2) from 0.24 ns to 4.62 ns confirms the defect passivation by lecithin molecules. While lecithin reduces the perovskite grain size, it improves surface coverage which enhances the shunt resistance, thereby increasing the carrier lifetime. As a result, despite smaller grains, the TRPL data still indicate longer carrier lifetimes.

From dark *J–V*, shunt resistance, TRPL, XRD and SEM analyses, the primary role of lecithin is to improve the uniformity and compactness of the very thin $CsPbBr_3$ films. The shunt resistance increased from $(1.3 \pm 0.1) \times 10^5\ \Omega$ to $(1.7 \pm 0.4) \times 10^5\ \Omega$, while the leakage current in devices fabricated with 3% lecithin precursor solution was approximately 40 times lower than that of pristine $CsPbBr_3$ cells. These improvements are consistent with more homogeneous and defect-suppressed films. Additionally, previous studies on perovskite LEDs have also suggested that lecithin interacts with $CsPbBr_3$ and passivates grain boundaries, providing evidence through FTIR, Tyndall effect, and photoluminescence analyses [39]. In our present work, we extend this understanding by providing complementary XPS analysis (absent in the previous LED study) which further supports the grain-boundary passivation mechanism.

XPS analysis of the Pb 4f region shows the characteristic Pb^{2+} doublet at ∼138.30/143.20 eV for the pristine $CsPbBr_3$ film and ∼138.31/143.15 eV for the lecithin-doped film (figure S6). The small binding-energy shift (⩽0.06 eV) confirms that Pb remains predominantly Pb^{2+} in both cases, indicating no change in lattice composition which is consistent with our XRD results too. In the control spectrum, a low-binding-energy shoulder at ∼136.9/141.8 eV corresponds to metallic Pb^0 species, typically associated with under-coordinated Pb at surfaces or grain boundaries [60]. This Pb^0 component becomes weak or non-resolvable in the lecithin-doped film, while the main Pb^{2+} peaks broaden slightly (FWHM 4 $f_{7/2}$: 1.46 to 1.59 eV) and total Pb 4f area decreases by ∼20%. These features indicate that lecithin coordinates with under-coordinated Pb, suppressing metallic-Pb sites at or near grain boundaries. A faint high-binding-energy shoulder (∼138.7–138.9 eV) emerges, consistent with Pb^{2+} in a more ionic or ligand-bound environment (e.g., Pb-phosphate coordination) [23, 61]. Together, these results add confirmation that lecithin interacts primarily at surface/grain-boundary regions, passivating Pb-related defects without altering the perovskite lattice structure as shown also in previous literature relating to $CsPbBr_3$ based LEDs and nanocrystals [37, 39].

The (95 ± 25) nm thickness of the $CsPbBr_3$ films makes our stacks very transparent to the visible region (figure 3) with AVT of 72.9% and CRI of 76.4%, calculated from equations [42], although limiting its light-harvesting capabilities and overall efficiencies [62]. We also produced fully transparent 3% lecithin solar cells replacing gold contacts with ITO (figure 5(e)). For these cells, AVT was 70.9% and CRI 83.5% (with a maximum PCE of 0.67%) (Table I). The lower PCE of ITO devices compared to

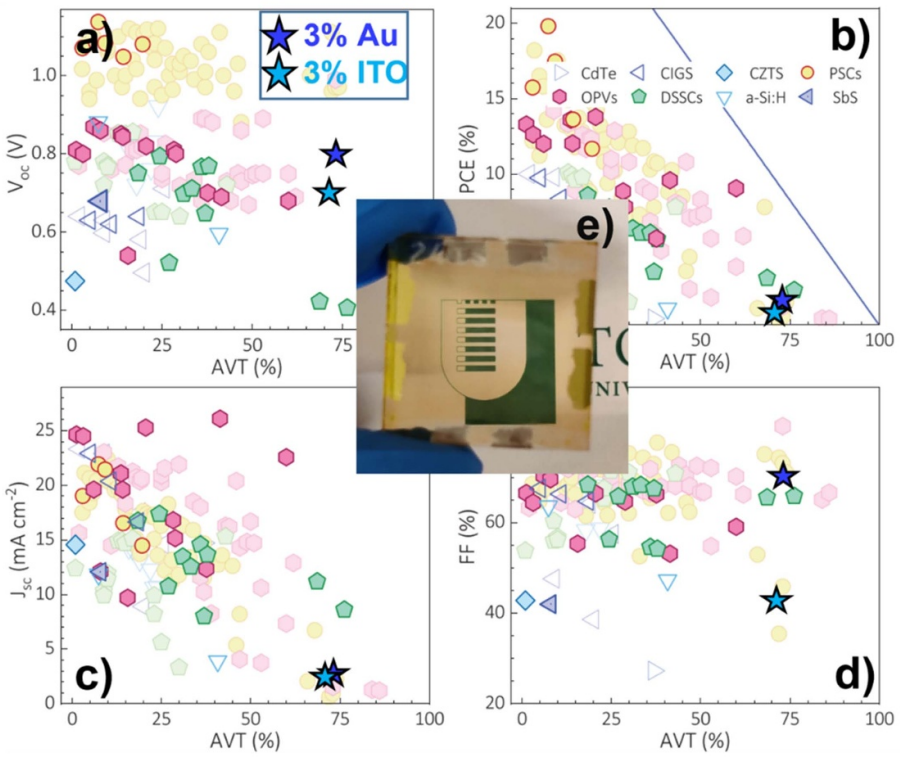

Figure 5. Best performing transparent and semitransparent PVs in literature adapted from [11]. The stars correspond to our best solar cells with 3% lecithin incorporation in precursor ink: the light blue stars for the device with ITO cathode and the dark blue stars for the one with gold (in this case AVT does not consider Au contribution). (a) Open circuit voltage, (b) power conversion efficiency, (c) short-circuit current density, (d) fill factor as a function of average visible transmittance. (e) Photograph of glass/FTO/c–TiO_2/m–TiO_2/$CsPbBr_3$ + lecithin/Spiro-OMeTAD/ITO solar cell. [11] John Wiley & Sons. © 2022 The Authors. Advanced Energy Materials published by Wiley-VCH GmbH.

opaque ones is related to the destructive process of the ITO sputtering. We estimate that replacing the sputtering procedure with a lower-energy alternative as well as inserting buffer layer such as MoOx or other suitable protective interlayers prior to ITO deposition [63–65] it would be possible to obtain PCEs within 10% in relative terms to those with metallic contacts.

Figure 5 is added in the manuscript to compare our device performance with values reported in the literature. Our photovoltaic (PV) parameters, including PCE, align well with those reported in a comprehensive literature survey covering various PV technologies [11] for highly transparent cells with AVT greater than 70%. When transparency exceeds 70%, most reported devices show PCEs $\sim$ 1% [10, 11]. In this context, our device achieves an AVT of 73% and a PCE of 1.52%, reflecting the intrinsic trade-off between transparency and light harvesting performance. Although PCEs are limited considerably by transparency (resulting in low photo-currents), V_{OC} are amongst the highest reported ($\geqslant$ 0.7 V) at these AVT levels [11] (figure 5(a)). This makes our devices particularly promising for low-energy applications such as powering internet of things devices [66].

Figure 6 shows the CIE 1931 chromaticity coordinates of our transparent ITO device stack showing very good color neutrality (with chromaticity coordinates of $x = 0.38$, $y = 0.39$). Color neutrality is a sought property for semitransparent applications that do not want to tint with color the visual sensation. The CRI of 84% is considered good color rendering, above the one required by the European standard EN 12 464–1 for workplaces ensuring adequate color fidelity for visual tasks [67]. The high AVT (>70%) and color neutrality makes our $CsPbBr_3$ solar cells suited for diverse applications that require low power, including lenses for smart glasses [68] (able at the same time to provide energy as well as blocking great part of UV and blue light [8] which is hazardous to eye health [69]), windows and building façades for BIPV [70], and greenhouses since wavelengths at $\sim$440 nm and 620–700 nm are the ones that contribute mostly to photosynthesis [71]. Furthermore, soy lecithin is naturally derived and considered non-toxic (here we used the readily available food product), environmentally friendly, and biodegradable, making it an additive of choice for photovoltaic bioelectronics [30, 72], and transient electronics applications [73].

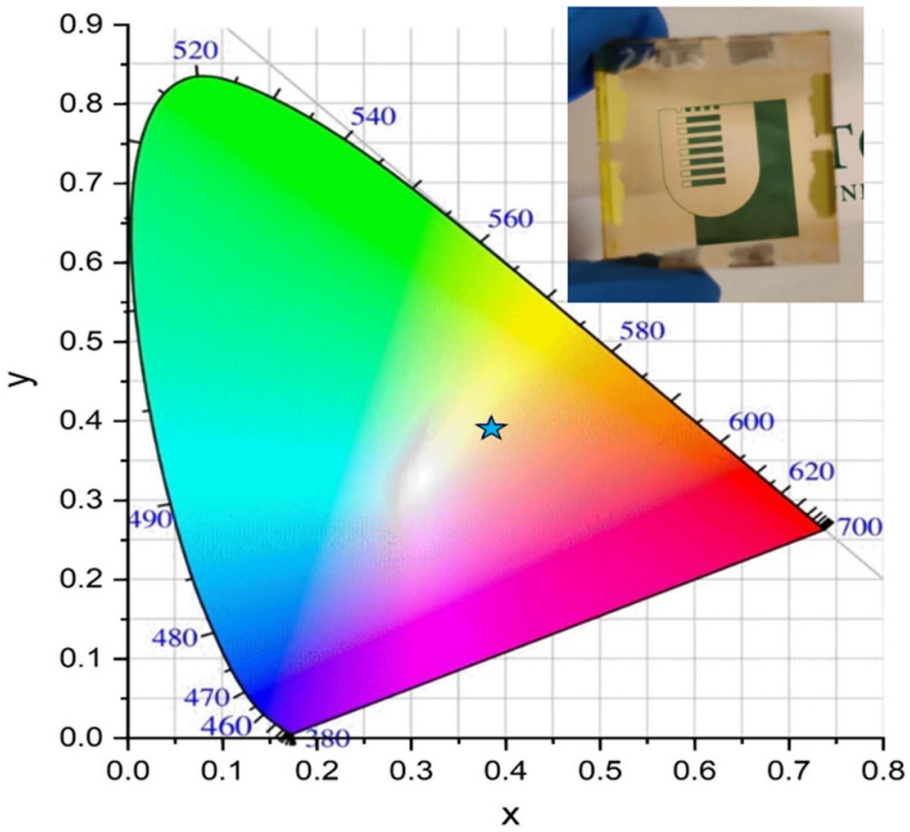

Figure 6. Photograph of glass/FTO/c–TiO_2/m–TiO_2/$CsPbBr_3$ + lecithin/Spiro-OMeTAD/ITO perovskite solar cell with top ITO electrode showing good color neutrality and a color rendering index of 84% (top right). The C.I.E. chromaticity diagram (main image) with the light blue star symbol indicating the chromaticity coordinates of the same cell at 0.38, 0.39.

4. Conclusions

We introduced soybean lecithin, a biological plant-based food additive, in the precursor ink that enabled to obtain higher quality of these very thin films $CsPbBr_3$ compared to those without. Solar cells fabricated for the first time with these films containing lecithin additive delivered PCEs of 1.52% compared to 0.84% those without. The stability in ambient air also improved with addition of lecithin, losing only 25% of efficiency after 1 year versus 50% for devices with no lecithin. The transparency of these films were high with AVTs (>70%) which limited photocurrents and thus efficiencies but consistent with literature results of highly transparent devices. Open circuit voltages were high ($\sim$ 0.8 V). The properties associated with CRI of 84% and neutrality (CIE coordinates of 0.38, 0.39) can enable the use in future applications where transparency and color neutrality are important features, such as windows, facades, lens in smart glasses, and greenhouses.

Note: during preparation of the second revised version of this manuscript, a study utilizing lecithin as a precursor additive was published showing improvement of the coverage of perovskite films on hydrophobic hole transport films in *p–i–n* architectures showing that it is effective when used with conventional organic-inorganic lead halide perovskites, delivering efficiencies of over 20% [74]. Our present work, submitted previously, demonstrates that the use of soybean lecithin food product is effective as an additive in *n–i–p* architectures and with fully inorganic $CsPbBr_3$ (semi-transparent) PSCs .Thus, the findings of this work and that of [74] combined, reveal soybean lecithin as an additive with more general effectiveness, delivering improvements over different perovskite formulations and device architectures.

Data availability statement

The data cannot be made publicly available upon publication because no suitable repository exists for hosting data in this field of study. The data that support the findings of this study are available upon reasonable request from the authors.

Acknowledgment

This work was supported by Italian Ministry of Research (MUR) through PRIN2022 REPLACE (project no. 2022C4YNP8) grant, from Lazio Region through ISIS@MACH (IR approved by Giunta Regionale no. G10795, 7 August 2019 published by BURL no. 69 27 August 2019), and the Air Force Office of Scientific Research's Biophysics program through awards n. FA9550-24-1-0320, FA9550-20-1-0157 and FA9550-25-1-0361. The authors acknowledge Mr. Zohair Abbas for his assistance with TiO_2 coating process.

ORCID iDs

Diksha Thakur 0000-0003-1633-653X
Aldo Di Carlo 0000-0001-6828-2380
Thomas M Brown 0000-0003-2141-3587

References

[1] Wu T *et al* 2021 The main progress of perovskite solar cells in 2020–2021 *Nanomicro Lett.* **13** 1–18
[2] Castro-Hermosa S, Dagar J, Marsella A and Brown T M 2017 Perovskite solar cells on paper and the role of substrates and electrodes on performance *IEEE Electron Device Lett.* **38** 1278–81
[3] Correa-Baena J-P, Saliba M, Buonassisi T, Grätzel M, Abate A, Tress W and Hagfeldt A 2017 Promises and challenges of perovskite solar cells *Science* **358** 739–44
[4] Ullah S *et al* 2021 All-inorganic CsPbBr3perovskite: a promising choice for photovoltaics *R. Soc. Chem.* **21** 646–83
[5] Wang J-K, Hou H-Y, Li Y-Q and Tang J-X 2020 Recent advances in interface engineering of all-inorganic perovskite solar cells *Nanoscale* **12** 17149–64
[6] Zhang X, Qian Y, Ling X, Wang Y, Zhang Y, Shi J, Shi Y, Yuan J and Ma W 2020 α-$CsPbBr_3$ perovskite quantum dots for application in semitransparent photovoltaics *ACS Appl. Mater. Interfaces* **12** 27307–15
[7] Gupta S, Kulbak M and Cahen D 2020 Pin-hole-free, homogeneous, pure $cspbbr_3$ films on flat substrates by simple spin-coating modification *Front. Energy Res.* **8** 504500
[8] Chen W *et al* 2018 A semitransparent inorganic perovskite film for overcoming ultraviolet light instability of organic solar cells and achieving 14.03% efficiency *Adv. Mater.* **30** 1800855
[9] Barichello J *et al* 2025 Energy, and undefined 2025, 'exploiting the impact of ionic liquids and light exposure on performance of fully inorganic $CsPbBr_3$ semi-transparent perovskite solar cells *Sol. Energy* **287** 113237
[10] Liu T, Zhao X, Wang P, Burlingame Q C, Hu J, Roh K, Xu Z, Rand B P, Chen M and Loo Y-L 2023 Highly transparent, scalable, and stable perovskite solar cells with minimal aesthetic compromise *Adv. Energy Mater.* **13** 2200402
[11] Almora O *et al* 2023 Device performance of emerging photovoltaic materials (version 3) *Adv. Energy Mater.* **13** 2203313
[12] Zhang J, Hodes G, Jin Z and Liu S 2019 All-inorganic $CsPbX_3$ perovskite solar cells: progress and Prospects *Angew. Chem. Int. Ed.* **58** 15596–618
[13] Liu X, Tan X, Liu Z, Ye H, Sun B, Shi T, Tang Z and Liao G 2019 Boosting the efficiency of carbon-based planar $CsPbBr_3$ perovskite solar cells by a modified multistep spin-coating technique and interface engineering *Nano Energy* **56** 184–95
[14] Zhou L *et al* 2024 Tailored buried layer passivation toward high-efficiency carbon based all-inorganic $CsPbBr_3$ perovskite solar cell *Chem. Eng. J.* **496** 154043
[15] Wang D *et al* 2020 Highly efficient $CsPbBr_3$ planar perovskite solar cells via additive engineering with NH4SCN *ACS Publ.* **12** 10579–87
[16] Cheng L P *et al* 2019 Efficient $CsPbBr_3$ perovskite light-emitting diodes enabled by synergetic morphology control *Adv. Opt. Mater.* **7** 1801534
[17] Aranda C A, Alvarez A O, Chivrony V S, Das C, Rai M and Saliba M 2024 Overcoming ionic migration in perovskite solar cells through alkali metals *Joule* **8** 241–54
[18] Li Y, Duan J, Yuan H, Zhao Y, He B and Tang Q 2018 Lattice modulation of alkali metal cations doped $Cs_{1-x}R_xPbBr_3$ halides for inorganic perovskite solar cells *Solar RRL* **2** 1800164
[19] Tan S, Shi J, Yu B, Zhao W, Li Y, Li Y, Wu H, Luo Y, Li D and Meng Q 2021 Inorganic ammonium halide additive strategy for highly efficient and stable $CsPbi_3$ perovskite solar cells *Adv. Funct. Mater.* **31** 2010813
[20] Liu S, Guan Y, Sheng Y, Hu Y, Rong Y, Mei A and Han H 2020 A review on additives for halide perovskite solar cells *Adv. Energy Mater.* **10** 1902492
[21] Zhang W, Liu H, Qu Y, Cui J, Zhang W, Shi T and Wang H-L 2024 B-site co-doping coupled with additive passivation pushes the efficiency of pb–sn mixed inorganic perovskite solar cells to over 17% *Adv. Mater.* **36** 2309193
[22] Wang G, Chang J, Bi J, Zhang W and Meng F 2022 organic additive engineering to grow high-quality inorganic $CsPbx_3$ perovskite films for efficient and stable solar cells *Solar RRL* **6** 2200656
[23] Thakur D *et al* 2021 Structural, optical and excitonic properties of urea grading doped $CH_3NH_3PbI_3$ thin films and their application in inverted-type perovskite solar cells *J. Alloys Compd.* **858** 157660
[24] Thakur D, Chiang S-E, Yang M-H, Wang J-S and Chang S H 2022 Self-stability of un-encapsulated polycrystalline $MAPbI_3$ solar cells via the formation of chemical bonds between C60 molecules and MA cations *Sol. Energy Mater. Sol. Cells* **235** 111454
[25] Thakur D, Chiang S-E, Sevilla R, Yuan C-T, Chang S H and Tai C-Y 2023 Thiourea small molecules regulated slow passivation in $MAPbI_3$ thin films for enhanced stability and performance of perovskite solar cells *J. Phys. Chem. C* **127** 14914–23
[26] Islam A, Usman K, Haider Z, Alam M F, Nawaz A and Sonar P 2023 Biomass-derived materials for interface engineering in organic/perovskite photovoltaic and light-emitting devices *Adv. Mater. Technol.* **8** 2201390
[27] Zhu H, Wang H, Zhang Y and Li Y 2023 Biophotovoltaics: recent advances and perspectives *Biotechnol. Adv.* **64** 108101
[28] Cavinato L M, Fresta E, Ferrara S and Costa R D 2021 Merging biology and photovoltaics: how nature helps Sun-Catching *Adv. Energy Mater.* **11** 2100520

[29] Yoon J, Hou Y, Knoepfel A M, Yang D, Ye T, Zheng L, Yennawar N, Sanghadasa M, Priya S and Wang K 2021 Bio-inspired strategies for next-generation perovskite solar mobile power sources *Chem. Soc. Rev.* **50** 12915–84
[30] Joseph E *et al* 2024 Photovoltaic bioelectronics merging biology with new generation semiconductors and light in biophotovoltaics photobiomodulation and biosensing *npj Biosens.* **1** 15
[31] Li M, Zhou J, Tan L, Li H, Liu Y, Jiang C, Ye Y, Ding L, Tress W and Yi C 2022 Multifunctional succinate additive for flexible perovskite solar cells with more than 23% power-conversion efficiency *Innovation* **3** 100310
[32] Hou Y, Wang K, Yang D, Jiang Y, Yennawar N, Wang K, Sanghadasa M, Wu C and Priya S 2019 Enhanced performance and stability in DNA-perovskite heterostructure-based solar cells *ACS Energy Lett.* **4** 2646–55
[33] Dagar J, Scarselli M, De Crescenzi M and Brown T M 2016 Solar cells incorporating water/alcohol-soluble electron-extracting DNA nanolayers *ACS Energy Lett.* **1** 510–5
[34] Dagar J, Scavia G, Scarselli M, Destri S, De Crescenzi M and Brown T M 2017 Coating ZnO nanoparticle films with DNA nanolayers for enhancing the electron extracting properties and performance of polymer solar cells *Nanoscale* **9** 19031–8
[35] Liu J, He Q, Bi J, Lei M, Zhang W and Wang G 2021 Remarkable quality improvement of $CsPbIBr_2$ perovskite film by cellulose acetate addition for efficient and stable carbon-based inorganic perovskite solar cells *Chem. Eng. J.* **424** 130324
[36] Cheng J and Dong J 2024 Isobutyramide additive to improve the performance of $CsPbBr_3$ perovskite solar cells prepared by green solvent *Phys. Status Solidi a* **221** 2400001
[37] Krieg F *et al* 2019 Stable ultraconcentrated and ultradilute colloids of $CsPbX_3$ (X = Cl, Br) nanocrystals using natural lecithin as a capping ligand *J. Am. Chem. Soc.* **141** 19839–49
[38] Milanese S, Morello G, De Giorgi M L, Cretì A, Andrusiv H, Bodnarchuk M I, Qualtieri A, Lomascolo M, Kovalenko M V and Anni M 2023 Air-sensitive amplified spontaneous emission in lecithin-capped $CsPbBr_3$ nanocrystals thin films *Mater. Today Phys.* **35** 101098
[39] Sun S-Q, Hua X-C, Liu Q-W, Wang T-T, Luo W, Zhang Y-J, Liao L-S and Fung M-K 2019 Influence of a lecithin additive on the performance of all-inorganic perovskite light-emitting diodes *J. Mater. Chem. C* **7** 2905–10
[40] Mir W J *et al* 2022 Lecithin capping ligands enable ultrastable perovskite-phase $CsPbI_3$ quantum dots for rec. 2020 bright-Red light-emitting diodes *J. Am. Chem. Soc.* **144** 13302–10
[41] Matteocci F, Rossi D, Castriotta L A, Ory D, Mejaouri S, der Maur M A, Sauvage F, Cacovich S and Di Carlo A 2022 Wide bandgap halide perovskite absorbers for semi-transparent photovoltaics: from theoretical design to modules *Nano Energy* **101** 107560
[42] Yang C, Liu D, Bates M, Barr M C and Lunt R R 2019 How to accurately report transparent solar cells *Joule* **3** 1803–9
[43] Singh P and Ravindra N M 2012 Analysis of series and shunt resistance in silicon solar cells using single and double exponential models *Emerg. Mater.* **1** 33–38
[44] Choi H, Choi K, Choi Y, Kim T, Lim S and Park T 2020 A review on reducing grain boundaries and morphological improvement of perovskite solar cells from methodology and material-based perspectives *Small Methods* **4** 1900569
[45] Khenkin M V *et al* 2020 Consensus statement for stability assessment and reporting for perovskite photovoltaics based on ISOS procedures *Nat. Energy* **5** 35–49
[46] Sardar R H, Bera A, Chattopadhyay S, Ali S I, Pramanik S and Mandal A C 2024 The impact of series (Rs) and shunt resistances (Rsh) on solar cell parameters to enhance the photovoltaic performance of f-PSCs *Opt. Mater.* **155** 115818
[47] Kulbak M, Cahen D and Hodes G 2015 How important is the organic part of lead halide perovskite photovoltaic cells? efficient $CsPbBr_3$ cells *J. Phys. Chem. Lett.* **6** 2452–6
[48] Liu Z, Sun B, Liu X, Han J, Ye H, Shi T, Tang Z and Liao G 2018 Efficient carbon-based $CsPbBr_3$ inorganic perovskite solar cells by using cu-phthalocyanine as hole transport material *Nano-Micro Lett.* **10** 34
[49] Rogdakis K and Kymakis E 2023 Interface engineering toward efficient carbon-based perovskite solar cells *Device* **1** 100123
[50] Chang X, Li W, Zhu L, Liu H, Geng H, Xiang S, Liu J and Chen H 2016 Carbon-based $CsPbBr_3$ perovskite solar cells: all-ambient processes and high thermal stability *ACS Appl. Mater. Interfaces* **8** 33649–55
[51] Zhao Y, Wang S, Ran H, Zhang Y and Tang Y 2023 Two-in-one additive engineering strategy induced high-quality $CsPbBr_3$ film in printable mesoscopic perovskite solar cells *J. Alloys Compd.* **965** 171317
[52] Ahn N, Son D-Y, Jang I-H, Kang S M, Choi M and Park N-G 2015 Highly reproducible perovskite solar cells with average efficiency of 18.3% and best efficiency of 19.7% fabricated via Lewis base adduct of lead (II) iodide *J. Am. Chem. Soc.* **137** 8696–9
[53] Bai S *et al* 2019 Planar perovskite solar cells with long-term stability using ionic liquid additives *Nature* **571** 245–50
[54] Toso S, Baranov D, Giannini C, Marras S and Manna L 2019 Wide-angle x-ray diffraction evidence of structural coherence in $CsPbBr_3$ nanocrystal superlattices *ACS Mater. Lett.* **1** 272–6
[55] Monshi A, Foroughi M R and Monshi M R 2012 Modified scherrer equation to estimate more accurately nano-crystallite size using XRD *World J. Nano Sci. Eng.* **02** 154–60
[56] Al-Taweel S *et al* 2016 New route for synthesis of pure anatase TiO2 nanoparticles via utrasound-assisted sol-gel method *J. Chem. Pharm. Res.* **8** 620–6 (available at: www.academia.edu/download/59347503/new-route-for-synthesis-of-pure-anatase-tio2-nanoparticles-via-utrasoundassisted-solgel-method_320190521-64109-1e8suv8.pdf)
[57] Xu J, Reddy S H, Castriotta L A, Podapangi S K, Luce M, Cricenti A, Di Carlo A and Brown T M 2023 30% efficient triple-cation perovskite solar cells under indoor illumination enabled by rare earth EuCl 3 doping *Sustain. Energy Fuel* **7** 3404–11
[58] Skafi Z *et al* 2023 Highly efficient flexible perovskite solar cells on polyethylene terephthalate films via dual halide and low-dimensional interface engineering for indoor photovoltaics *Solar RRL* **7** 2300324
[59] Kirchartz T, Márquez J A, Stolterfoht M and Unold T 2020 Photoluminescence-based characterization of halide perovskites for photovoltaics *Adv. Energy Mater.* **10** 1904134
[60] Wang S, Jiang Y, Juarez-Perez E J, Ono L K and Qi Y 2017 Accelerated degradation of methylammonium lead iodide perovskites induced by exposure to iodine vapour *Nat. Energy* **2** 1–8
[61] Shen X, Kang K, Yu Z, Jeong W H, Choi H, Park S H, Stranks S D, Snaith H J, Friend R H and Lee B R 2023 Passivation strategies for mitigating defect challenges in halide perovskite light-emitting diodes *Joule* **7** 272–308
[62] Mehrabian M, Dalir S, Mahmoudi G, Miroslaw B, Babashkina M G, Dektereva A V and Safin D A 2019 A highly stable all-inorganic $CsPbBr_3$ perovskite solar cell *Eur. J. Inorg. Chem.* **2019** 3699–703
[63] Magliano E, Mariani P, Agresti A, Pescetelli S, Matteocci F, Taheri B, Cricenti A, Luce M and Di Carlo A 2023 Semitransparent perovskite solar cells with ultrathin protective buffer layers *ACS Appl. Energy Mater.* **6** 10340–53
[64] Pan J *et al* 2025 Optimization of the MoOX buffer layer for single-junction and four-terminal perovskite–silicon tandem solar cells *J. Mater. Chem. A* **13** 32169–78
[65] Aydin E *et al* 2021 Sputtered transparent electrodes for optoelectronic devices: induced damage and mitigation strategies *Matter* **4** 3549–84

[66] Chakraborty A et al 2024 Photovoltaics for indoor energy harvesting Nano Energy 128 109932
[67] CEN (European Committee for Standardization) 2021 EN 12464–1:2021—light and lighting—lighting of work places—Part 1: indoor work places (European Standard) (available at: www.ageta.lt/app/webroot/files/uploads/filemanager/File/info/EN_12464-1')
[68] Landerer D, Bahro D, Röhm H, Koppitz M, Mertens A, Manger F, Denk F, Heidinger M, Windmann T and Colsmann A 2017 Solar glasses: a case study on semitransparent organic solar cells for self-powered, smart, wearable devices Energy Technol. 5 1936–45
[69] Delic N C, Lyons J G, Di Girolamo N and Halliday G M 2017 Damaging effects of ultraviolet radiation on the cornea Photochem. Photobiol. 93 920–9
[70] Lee K et al 2020 The development of transparent photovoltaics Cell Rep. Phys. Sci. 1 100143
[71] Mashkov P H, Beloev H I, Gyoch B S, Kandilarov R Y and Pencheva T G 2017 LED equipment for light influence on photosynthesis investigations 2017 XXVI Int. Scientific Conf. Electronics (ET) vol 2017 pp 1–4
[72] Bhatnagar P, Patel M, Nguyen T T, Kim S and Kim J 2021 Transparent photovoltaics for self-powered bioelectronics and neuromorphic applications J. Phys. Chem. Lett. 12 12426–36
[73] Ding Z, Qiao J, Gao W-C, Wang C and Guan Y-S 2025 A comprehensive review on biodegradable materials and technologies for transient electronics Adv. Mater. Technol. e01928
[74] Chen Q et al 2025 Soybean lecithin as a passivator and compatibilizer in p-i-n perovskite solar cells ACS Appl. Mater. Interfaces 17 44481–9